Bioactive glass-derived trabecular coating: a smart solution for enhancing osteointegration of prosthetic elements

Bioactive glass-derived trabecular coating: a smart solution for enhancing osteointegration of prosthetic elements

Chiara Vitale-Brovarone*, Francesco Baino, Francesca Tallia, Cristina Gervasio, Enrica Verné

Institute of Material Engineering and Physics, Applied Science and Technology Department, Politecnico di Torino, Corso Duca degli Abruzzi 24, 10129 Torino, Italy.

* Corresponding author: Chiara Vitale-Brovarone

Phone: +39 011 090 4716

Fax: +39 011 090 4699

E-mail: chiara.vitale@polito.it

Abstract

In this work, the use of foam-like glass-ceramic scaffolds as trabecular coatings on ceramic prosthetic devices to enhance implant osteointegration is proposed. The feasibility of this innovative device was explored in a simplified, flat geometry: glass-ceramic scaffolds, prepared by polymeric sponge replication and mimicking the trabecular architecture of cancellous bone, were joined to alumina square substrates by a dense glass coating (interlayer). The role played by different formulations of starting glasses was examined, with particular care to the effect on the mechanical properties and bioactivity of the final coating. Microindentations at the coating/substrate interface and tensile tests were performed to evaluate the bonding strength between the sample's components. *In vitro* bioactive behaviour was assessed by soaking in simulated body fluid and evaluating the apatite formation on the surface and inside the pores of the trabecular coating. The concepts disclosed in the present study can have a significant impact in the field of implantable devices, suggesting a valuable alternative to traditional, often invasive bone-prosthesis fixation.

Keywords: Bioactive glass; Coating; Prosthesis; Osteointegration; Scaffold.

1. Introduction

Over the last two decades, the approach towards an optimal fixation of orthopaedic and dental implants changed and evolved towards "bone-conservative" solutions [1,2]. Specifically, the researchers' attention progressively moved from simple mechanical fixation to host tissue(s), which involves the use of screws, threaded implants or polymeric cements, towards a physico-chemical bond able to minimize bone resection/loss and maximize implant osteointegration. This goal can be achieved by coating the implant with a bioactive material, that also allows to protect the substrate from corrosion or degradation by biological fluids and agents, which is a crucial issue especially for metal implants [3].

From a general viewpoint, bioceramic coatings can be manufactured by a wide variety of methods, including gravity-controlled deposition [4-8], sol-gel dipping [9], spin coating [10], plasma spraying [11], sputtering [12] and electrophoretic deposition [13]. At present, the most accepted and commercialized bioceramic coating is thermally sprayed hydroxyapatite (HA) [11]. HA coatings can promote faster and stronger bonding to bone in comparison with the loosely adherent layer of fibrous tissue at the implant interface in other cementless fixation, but exhibit a durability that is strongly related to coating properties, such as microstructure, surface texture and presence of pores/cracks that can vary greatly [11,14,15]. In fact, control of variables in plasma spraying is quite complicated and, therefore, small changes to processing variables can vastly affect the properties of the final coating. Furthermore, noticeable problems of HA coatings are due to material thermal instability: high processing temperatures might induce HA decomposition into soluble calcium phosphate compounds, that undergo undesired fast resorption *in vivo* [14].

Several researchers proposed bioactive glasses as a promising alternative to HA to manufacture coatings on prosthetic implants [3-7,9,10,16]. It was widely demonstrated that bioactive silicate glasses are able to strongly bond to bone creating a stable interface [17,18] and their dissolution products have a stimulatory effects on the genes of cells towards a path of tissue regeneration and angiogenesis [19,20]. An interesting challenge of tissue engineering concerns the compositional design of bioactive glass coatings in order to induce specific cell responses at the genetic level [21]. From a manufacturing

viewpoint, fabrication of high-quality glass coatings on both metal and ceramic elements is a complex issue due to poor coating adhesion and/or glass degradation during the coating procedure, which eventually ensues in unsatisfactory mechanical properties. In such a context, Verné and co-workers [4,6,7] and Tomsia and co-workers [5,16,21] dedicated significant efforts over the last ten years to optimize glass compositions and processing parameters to obtain bioactive coatings with high adhesion strength. Tomsia et al. [16] also emphasized the potential of graded glass or glass/HA coatings, in an attempt to obtain excellent adhesion at the coating-implant interface and high bioactive properties of coating surface. Apart from being used to manufacture coatings, bioactive glasses are often designed to act as porous templates (scaffold) to enhance tissue regeneration and in-growth [22,23]. In this case, structural bio-mimicry of scaffold with respect to cancellous bone and morpho-architectural effect – it is known that tissue in-growth is favoured by a porous structure *per se* [24] – are coupled to the tissue regenerative potential of the glass due to its bioactivity [17,18].

In this article, we merged the concepts of bioactive coating and bone-like scaffold to investigate the feasibility of highly innovative glass-derived trabecular coatings on alumina substrates. This novel class of coatings represents a significant advance over traditional, dense coatings; the basic idea of the research was disclosed in a patent recently deposited by the authors [25]. Referring to the context of hip joint prosthesis, the authors proposed a monoblock acetabular cup that can be anchored to the patient's bone without using either cement or metal-back, but by means of a bioactive trabecular coating able to promote implant osteointegration (Fig. 1). The "driving force" of this work can be resumed in the motto "*Naturae imitatio*", as the authors' goal was to develop a bioactive coating to be lastly used on prosthetic devices that closely mimicked the 3-D pore architecture of cancellous bone, thereby enhancing bone in-growth and ensuring a stable anchorage of the implant to host bone thanks to its porous network and bioactive properties.

2. Materials and methods

2.1. Starting materials

2.1.1. Preparation

High-purity (> 99.5%) dense alumina 1-mm thick sheets (Goodfellow, Cambridge, UK) were used as ceramic substrates for fabricating all the samples described in this work. Alumina sheets were cut by means of a rotating diamond wheel (Accutom 5 Machine, Struers) to obtain square 10 mm × 10 mm plates.

The glasses used in this work are listed in Table 1; they all were prepared by melting the raw products in a platinum crucible in air and then by quenching the melt in cold water to obtain a "frit", that was subsequently ground by a 6-balls zirconia milling and eventually sieved by stainless steel sieves (Giuliani Technologies, Italy) to the desired particle size. For reader's better understanding, it is worth anticipating here that all glasses used in this work will be converted, by high-temperature thermal treatments, into glass-ceramic (GC) materials.

2.1.2. Characterization

SCK [6] and CEL2 [26,27] were studied by the authors in previous reports; the characterization of SCNA is reported in detail in the present work as it was only partly investigated elsewhere for other biomedical applications [28].

As-poured SCNA underwent wide-angle (2θ within 10-70°) X-ray diffraction analysis (XRD) by using a X'Pert diffractometer (Bragg-Brentano camera geometry with Cu Kα incident radiation; working conditions: 40 kV, 30 mA).

The behaviour of compacts of SCNA powders upon heating was monitored by hot-stage microscopy (HSM) (Expert System Solutions instrument) performed in air atmosphere; HSM set-up is described elsewhere in detail [29].

Differential thermal analysis (DTA) was carried out on SCNA by using a DTA7 Perkin-Elmer instrument; experimental set-up is described elsewhere in detail [29]. The characteristic temperatures of

the material, i.e. glass transition temperature (T_g), onset crystallization temperature (T_x) and peak crystallization temperature (T_c), were assessed directly from the DTA plots.

Linear thermal expansion coefficient (α) of SCK, CEL2 and SCNA were calculated from their molar compositions (percentage of oxides) by using SciGlass Professional 7.3 software according to the method proposed by Priven [30].

2.2. Dense coating (interlayer)

2.2.1. Manufacturing

The dense coatings (interlayer) on alumina substrates were prepared via controlled deposition of SCK, CEL2 or SCNA powders (the 75-106 μm range for glass particles was selected as the optimal one) followed by thermal treatment. To manufacture dense coating, a suspension of glass powders in ethanol was poured onto the alumina plates placed in a beaker [6]; the glass powder had settled on the substrates overnight. By knowing the bottom area (A_b) of the beaker, the glass density (ρ_g) and the desired layer thickness (t), the mass (m) of glass necessary for the deposition can be easily calculated as $m = \rho_g A_b t$; the interlayer thickness was planned to be ~200 μm. The beaker was then placed in an oven at 90 °C for 6 h to remove the exceeding ethanol and to dry the "green" coating completely. Lastly, the so-prepared samples were thermally-treated under different conditions depending on the glass used to manufacture the coating (see the section 2.4.1.).

2.2.2. Characterization

The samples were embedded in epoxy resin, cut, carefully polished by #600 to #4000 SiC grit papers, silver-coated and finally investigated by scanning electron microscopy (SEM; Philips 525 M operating at 15 kV) equipped with electron dispersive spectrometer (EDS; Philips EDAX 9100) for compositional analysis.

The coatings also underwent wide-angle XRD analysis to detect the presence of crystalline phases after the thermal treatment.

Vickers indentation (HV) tests were performed at the interface between glass-derived dense coatings and alumina substrate in order to evaluate, from a qualitative viewpoint, the adhesion between the two materials. The indentations were made by means of a Leitz micro-Vickers penetrator using the maximum load (5 N) available for the instrument. The samples were incorporated in resin, cut and then carefully polished by #600 to #4000 SiC grit papers before the tests. An effective joining between coating and substrate should involve no propagation of cracks along the interface between the two different materials, which would lead to coating delamination [31,32].

Finally, in order to assess quantitatively the adhesion strength of the coatings, tensile tests were performed on the samples according to ASTM standards [33,34] by using a Syntech 10/D machine (MTS Corp.) with cross-head speed set at 1 mm min^{-1}. Briefly, each sample were glued to two loading fixtures (steel cylinders with a diameter of 16 mm) by using an epoxy resin (Araldite® AV 119, Ciba-Geigy) able to withstand a maximum stress of ~40 MPa (as declared by the manufacturer). At room temperature, the adhesive agent is a gel; its polymerization was achieved by a thermal treatment in oven (130 °C/1 h). The failure tensile stress σ_t (MPa) was calculated as $\sigma_t = \frac{L_t}{A_t}$, where L_t (N) is the breaking-off load and A_t (mm^2) is the resistant section area measured after the test.

2.3. Trabecular coating (scaffold)

2.3.1. Fabrication

Glass powders sieved below 32 μm were used as starting materials for scaffolds fabrication. GC-CEL2 and GC-SCNA scaffolds to be employed as trabecular coatings were produced through sponge replication method, according to a processing schedule described elsewhere [27]. Commercial open-cells polyurethane (PU) sponge (apparent density ~20 kg m^{-3}), used as a sacrificial templates, was

manually cut by a surgical scalpel in thin blocks (thickness ~4 mm) properly oversized with respect to the dimensions of the alumina plates (10 mm × 10 mm) that they should coat: this was necessary to take into account the scaffold volumetric shrinkage occurring due to sintering.

2.3.2. Characterization

Scaffolds structure and morphology were evaluated through SEM to assess pores size, shape and distribution.

The volumetric shrinkage S_v (%), due to the PU template removal and to the glass softening-sintering, was estimated by geometrical measurements before and after the thermal treatment as $S_v = \left(\frac{V_0 - V_s}{V_0}\right) \times 100$, where V_0 is the volume of the glass-coated sponge before the thermal treatment and V_s is the volume of the final scaffold.

The porosity content Π (%vol.) was calculated by geometrical weight-volume evaluations as $\Pi = \left(\frac{\rho_0 - \rho_s}{\rho_0}\right) \times 100$, where ρ_0 is the density of non-porous material and ρ_s is the density of the scaffold (weight/volume ratio including the contribution of the pores).

The scaffolds strength was evaluated through compressive tests (Syntech 10/D machine, cross-head speed set at 1 mm min^{-1}) on dry cubic ~10^3-mm^3 samples; the compressive strength σ_c (MPa) was obtained as $\sigma_c = \frac{L_c}{A_c}$, where L_c (N) is the maximum compressive load registered during the test and A_c (mm^2) is the resistant area perpendicular to the load axis [27].

In vitro tests were carried out by soaking the scaffolds in acellular simulated body fluid (SBF) prepared according to Kokubo's recipe [35]. Cubic ~10^3-mm^3 samples were soaked for 7 days and 1 month in 30 ml of SBF maintained at 37 °C; every 48 h the samples were gently washed with distilled water and the solution was replaced by fresh SBF to simulate fluid circulation in the human body. After soaking, the samples were dried at room temperature and then investigated through SEM and EDS.

2.4. Complete plane samples

2.4.1. Preparation

After manufacturing dense coatings on alumina plates and scaffolds, these two elements were joined together in order to obtain a complete sample that reproduced, in a simplified plane geometry, the device depicted in Fig. 1. Three different approaches, hereafter referred to as methods I, II and III, were followed to fabricate these "plane" samples (Fig. 2). The search for an ever increasing ease of processing, as well as the achievement of better results especially in terms of coating adhesion, was the leitmotiv driving the methods evolution.

By method I, coatings based on SCK particles (range within 75-106 μm) were manufactured on alumina plates via controlled deposition as described in the section 2.2.1. Afterwards, the green coating was directly introduced into a furnace at 1300 °C, thermally treated for 5 min and finally annealed at 650 °C for 3 h. On this SCK-derived layer, a second coating was manufactured via controlled deposition by using CEL2 powders in the 75-106 μm range; then, a GC-CEL2 scaffold, previously prepared as described in the section 2.3.1., was stacked on the green CEL2 coating and the whole system was thermally treated at 1000 °C for 3 h. Before the stacking procedure, the GC-CEL2 scaffold was carefully polished by SiC grit paper in order to smooth its surface in an attempt to improve its adhesion to the underlying layer. The presence of the green CEL2 layer between the SCK coating and the GC-CEL2 scaffold was expected to improve the adhesion at the GC-SCK coating/GC-CEL2 scaffold interface.

In method II the double coating was manufactured as well as reported in method I. A CEL2-impregnated sponge was stacked on the green CEL2 layer and the whole system was thermally treated at 1000 °C for 3 h (the CEL2 dense layer and CEL2-based trabecular coating were sintered at the same time).

With respect to methods I and II, in method III the samples manufacturing was simplified. Only one glass (SCNA) was used as starting material to prepare both the dense coating (interlayer) on alumina and the scaffold (trabecular coating). First, a SCNA green coating was prepared on the alumina plate and no thermal treatment of sintering was performed; afterwards, a SCNA-impregnated sponge was stacked on the green SCNA coating and, finally, the whole system was thermally treated at 1000 °C for 3 h (1-step thermal treatment).

In the light of the strict similarity between methods I and II, we will refer to them by the denotation "first embodiment", whereas method III will be referred to as "second embodiment".

2.4.2. Characterization

The samples were embedded in epoxy resin, cut, polished by #600 to #4000 SiC grit papers, silver-coated and investigated by SEM.

In vitro tests were also performed by soaking the samples in SBF, according to what was previously exposed in the section 2.3.2.

3. Results and discussion

3.1. Starting materials

In order to fabricate the SCK-, CEL2- and SCNA-derived coatings, the glass particles were sieved within 75-106 μm, whereas glass powders sieved below 32 μm were used for scaffolding.

Characterizations of SCK [6] and CEL2 [26,27,29] were previously reported by the authors; the results of SCNA investigation are included in the present work, as this glass was only partly analyzed elsewhere [28].

The characteristic temperatures of SCNA, assessed directly by the DTA plot (not shown), are T_g = 690 °C, T_x = 820 °C and T_c = 856 °C.

The glass-derived coatings and scaffolds obtained after treatment at 1000°C for 3 h were glass-ceramic (GC-SCNA), because a crystalline phase ($CaSiO_3$, wollastonite) developed during the thermal treatment (XRD data not reported); biocompatibility of wollastonite is known since the mid 1980s [36,37].

Previous studies showed that, after high-temperature treatments, also SCK [6] and CEL2 [26,27,29] are converted into glass-ceramic materials.

The α values of the three glasses used in this work are shown in Table 1.

3.2. First embodiment

3.2.1. Dense coating (interlayer)

As reported in the patent deposited by the authors [25], the presence of a glass-derived interlayer is necessary to increase the number of contact points and, accordingly, the bonding strength between alumina and trabecular coating. Although CEL2 was proved to have attractive features for biomedical use, [26,27,29], it appeared unsuitable to be used as a coating material on alumina since its α value (Table 1) was far from that of alumina (~8.5×10^{-6} °C^{-1}). A good α's "matching" between coating material (glass) and substrate (alumina) ensues in the fabrication of flawless, homogeneous and uniform coatings; therefore, also in the light of previous results [6], SCK was selected for producing the interlayer since its α value (Table 1) is closer to that of alumina.

SCK powders were sieved within three size ranges, i.e. below 32 μm, within 32-75 μm and within 75-106 μm, and then used to manufacture the coatings on small alumina plates. As clearly shown in Fig. 3a, the use of SCK particles below 32 μm led to unsatisfactory results (almost total absence of adhesion). SCK powders sieved within 32-75 μm were able to coat the alumina more uniformly, but the coating seemed to be divided in "islands" separated by cracks and void spaces (Fig. 3b). Finally, the coatings produced by using powders of larger size (Figs. 3c,d) were continuous and homogeneous; therefore, only glass particles within 75-106 μm were employed to manufacture the coatings. These results

confirm that glass particles size can influence the "quality" of the final glass-derived products (especially coatings), as shown in previous literature [29,38].

$CaSiO_3$ (wollastonite) was identified as the unique crystalline phase of GC-SCK in a previous work by the authors [6].

Fig. 4a shows the cross-section of the GC-SCK/GC-CEL2 interlayer after careful polishing; the SEM back-scattered mode, coupled with the compositional (EDS) analysis (Figs. 4b,c), allows of well distinguishing the different employed materials. The adhesion between GC-SCK coating and alumina is excellent, without any crack or defect at the interface, as well as the joining between GC-SCK and GC-CEL2 layers. It is possible to distinguish two different regions in the GC-SCK coating, characterized by two different grey levels emphasized in the back-scattered mode (Fig. 4a). The EDS pattern reported in Fig. 4c shows that the upper layer (light grey) is constituted by calcium (Ca) and silicon (Si); therefore, we can hypothesize the presence of wollastonite in such a region, also considering that this phase was detected in SCK-derived coatings after thermal treatment above 900 °C in a previous work [6]. As shown in Fig. 4b, the region in contact with alumina (dark grey) contained silicon (Si), calcium (Ca) and potassium (K), typical for SCK composition, sodium (Na) that might have migrated here from the GC-CEL2 layer, and aluminium (Al) that migrated here from the alumina substrate during the thermal treatment.

The thickness of the GC-SCK coating was in the 170-190 μm range (Fig. 4a), which is close to the theoretical value set by controlled deposition (200 μm): this demonstrates that the gravity-guided deposition is an easy, effective method to tailor the coating thickness.

Microindentations at the coating/substrate interface are commonly performed to evaluate the propagation of the cracks induced by the indenter, in order to preliminarily assess the "quality" of adhesion between the two materials [31]. Fig. 5 shows that the cracks did not propagate along GC-SCK/alumina interface, but rather tended to be driven into the glass-ceramic coating (the "weaker" material). The good adhesion between the two elements was probably enhanced by the enrichment in Al^{3+} ions of the coating region near to the alumina substrate (Fig. 4b), which caused a modification of

the α of the coating material towards a value closer to that of alumina, thereby reducing interfacial stresses.

3.2.2. Trabecular coating (scaffold)

In the light of the results reported elsewhere by the authors [26,27,29], CEL2 may be considered an attractive material for producing the trabecular coating, as GC-CEL2 scaffolds exhibit attractive properties (e.g. mechanical strength comparable to that of cancellous bone, excellent bioactivity and biological compatibility) that are not described here in detail to avoid data duplication.

3.2.3. Complete plane samples

Qualitative differences in terms of adhesion at the alumina/interlayer and interlayer/trabecular coating interfaces of the samples prepared by methods I and II were investigated by SEM. Fig. 6a shows that, in the sample produced by method I, the adhesion between trabecular coating and interlayer is limited to few contact areas, i.e. the regions where GC-CEL2 scaffold and CEL2 layer were effectively in contact before sintering. In the sample obtained by method II (Figs. 6b,c), the adhesion between the two elements was found to be qualitatively better, as the CEL2-impregnated sponge could adhere more effectively to the CEL2 coating lying underneath, thereby increasing the number of contact areas. Furthermore, it should be considered that the joining between interlayer and trabecular coatings is strongly promoted by viscous flow sintering, that occurred more conspicuously in the case of method II – contact between a glass (CEL2) layer and a glass (CEL2)-coated sponge – than in method I – contact between a glass (CEL2) layer and a pre-sintered glass-ceramic (GC-CEL2) scaffold.

The complete plane samples were tested in SBF to assess whether the alumina substrate might have a detrimental effect on *in vitro* bioactivity and, accordingly, on the osteointegrative potential of the proposed device. Fig. 7a shows that the treatment in SBF for 1 week does not seem to influence the adhesion at the various interfaces of the system (alumina/GC-SCK, GC-SCK/GC-CEL2, GC-

CEL2/scaffold). In addition, the scaffolds struts were completely coated by a thick layer (30-50 μm) of a newly formed phase that grew also on the walls of the inner pores of the scaffolds (Fig. 7b), thereby demonstrating that the pores network was characterized by high interconnection. Compositional analysis performed on this newly formed layer showed its apatitic nature, with Ca/P molar ratio equal to 1.70. After soaking for 1 month in SBF, sample integrity does not seem to be modified by the *in vitro* treatment. The thickness of the newly formed apatitic phase significantly increased over time reaching up to ~100 μm, that is above twice the thickness measured after soaking in SBF for 1 week only: in fact, its presence can be distinguished also in the low-magnification SEM micrograph reported in Fig. 7c (see the white circles and arrows). Ca/P molar ratio was equal to 1.68, which is very close to the Ca/P ratio (1.67) of stoichiometric HA.

3.3. Second embodiment

Although the feasibility of bioactive trabecular coatings on flat alumina substrates was successfully demonstrated by means of Methods I and II, such techniques required a multi-step processing schedule. Therefore, in view of a future transfer from "Lab-scale" to industrial application, the authors tried to simplify the fabrication process by adopting a single glass (SCNA) to manufacture both the dense interlayer and the trabecular coating. SCNA exhibited excellent coating ability on alumina (thanks to a good "α matching" between the two materials) and high-strength properties.

3.3.1. Dense coating (interlayer)

Dense GC-SCNA coatings were fabricated on square alumina plates via gravity-controlled deposition of glass powders sieved within 75-106 μm, as already optimized for SCK-derived coatings.

From a macroscopic viewpoint, GC-SCNA coatings were similar to those reported in Figs. 3c,d, i.e. they were well adherent to the alumina substrate and exhibited a uniform thickness. These observations were confirmed by SEM investigations; Fig. 8 shows, at different magnifications, the interface between

alumina and coating: the GC-SCNA layer is homogeneous with thickness of ~200 μm, in agreement with the planned value (Fig. 8a), and no pores or flaws can be observed at the interface between the two materials, even at high magnification (Fig. 8b). The glass-ceramic nature of the coating is clearly visible in Fig. 8b, as needle-shaped "white" crystals, identified as $CaSiO_3$ (wollastonite) and embedded in a "dark" amorphous matrix, are clearly distinguishable.

Microindentations at the interface were employed to estimate the "quality" of joining between coating and substrate: in Fig. 9 the arrows show a small crack that propagates only through the coating, without detaching it from alumina.

In order to obtain quantitative data on the GC-SCNA/alumina bonding strength, these plane coatings underwent tensile (adhesion) tests; failure stress was σ_t = 20.6 MPa (SD = 4.2 MPa). If we refer to international standards, a tensile stress of at least 15 MPa is recommended, for instance, in the case of HA coatings on titanium alloys [39]. Therefore, the adhesion strength obtained for the GC-SCNA coatings seems to be promising and suggests an actual mechanical suitability of the prepared material for biomedical use.

3.3.2. Trabecular coating (scaffold)

SCNA-derived scaffolds were fabricated by sponge replication method [27]; the sintering temperature for scaffolding (1000 °C) was chosen on the basis of HSM results.

Fig. 10 reports SEM micrographs of GC-SCNA scaffold showing that after the thermal treatment an excellent glass particles densification, as well as a satisfactory pores content, was successfully achieved. In Fig. 10a a bimodal distribution of scaffold pores – pores above 100 μm originated by the 3-D macro-cells network of the PU template and pores below 10 μm – is clearly evident. Both large and small pores are homogeneously distributed along the section, demonstrating that the density of the scaffold is homogeneous in its whole volume without gradients of porosity. In Fig. 10b the very good sintering of scaffold struts is still more evident than in Fig. 10a, since it is not possible to distinguish the original SCNA particles. Fig. 10c puts into evidence the typical needle-like shape of $CaSiO_3$ crystals (10-15 μm

in length) nucleated during sintering; the nature of these crystals was also confirmed by compositional analysis (EDS spectrum not shown).

The volumetric shrinkage assessed of GC-SCNA scaffolds was S_v = 62.3 % (SD = 1.6 %) and their total porosity was Π = 63.0 %vol. (SD = 1.3 %vol.), that is comparable to the pores content of natural cancellous bone (50-70%vol. [24]).

The mean compressive strength of GC-SCNA scaffolds was σ_c = 12.5 MPa (SD = 2.9 MPa); this value is more than twice higher than that obtained for GC-CEL2 scaffolds (5-6 MPa) with analogous porosity/architecture and manufactured by the same processing schedule [27]. The superior mechanical behaviour of GC-SCNA scaffolds can be ascribable to intrinsic material features, and more specifically to the different mechanical features of the crystalline phases nucleated in the two glass-ceramic materials. This hypothesis can be supported by following an approach based on the fact that, in principle, higher the density of a material, higher is its mechanical strength [29]. By comparing the densities of the crystalline phases detected by XRD in GC-SCNA and GC-CEL2 scaffolds, we observed that the density of $CaSiO_3$ (~2.92 g cm^{-3}) is higher than that of the major phase of GC-CEL2, $Na_4Ca_4(Si_6O_{18})$ (~2.85 g cm^{-3}), which accordingly involves different mechanical strength of the two scaffolds. In addition, it is known that the presence of alumina in a glass formulation can contribute to increase the mechanical resistance of the material [23]; in the case of GC-SCNA, alumina is contained in the residual amorphous phase ($CaSiO_3$ was the crystalline phase). By assuming Bioglass®-based scaffolds fabricated by sponge replication as a standard reference, the compressive strength of GC-SCNA scaffolds is significantly higher than that of glass-ceramic Bioglass®-based scaffolds (0.3-0.5 MPa with 89-92 %vol. porosity [40]; 1.3-2.5 MPa with 69-71 %vol. porosity [29]) and polymer-coated Bioglass®-derived scaffolds (1.0-1.5 MPa with 79-85 %vol. porosity [41]) reported up to now in the literature. This significant improvement of mechanical strength is due to both the composition of starting glass (SCNA vs. Bioglass®) and the optimization of processing schedule that led to sound, well-densified scaffold struts [29].

Unluckily, GC-SCNA scaffolds were characterized by only a slight bioactive behaviour. After 7 days of soaking in SBF, partial dissolution of the material and formation of very small, round-shaped CaP

particles on scaffold struts can be observed (Fig. 11); CaP agglomerates, however, did not grow in amount and thickness with the increase of soaking time and, accordingly, subsequent formation of a continuous and homogeneous apatite layer did not occur. The bioactive process is a sequence of ion-exchange phenomena occurring between scaffold material and biological fluids [17] and in the present case the partial substitution of Si^{4+} ions with Al^{3+} ones in the tetrahedral units of the Al_2O_3-rich residual glassy phase of GC-SCNA led to a chemically stable network less prone to react with the surrounding environment. These results are consistent with the observations reported by Kokubo and co-workers for Al_2O_3- and wollastonite-containing biomedical glass-ceramics [42]. High stability of the residual amorphous phase of GC-SCNA scaffold during soaking in SBF was confirmed by weight measurements: after 3-month immersion, weight loss of ~3.3% and porosity increment of ~2.8 %vol. were registered, which involved only a mild decrease of the mechanical strength (–15.0% after soaking for 3 months in SBF). Accordingly, also the solution pH variations were quite moderate (maximum ~7.8 after the early 48 h of soaking) with respect to the basal pH value of SBF (7.40); therefore, no cytotoxic effect due to pH increase is expected.

3.3.3. Complete plane samples

From a qualitative viewpoint, good adhesion at the alumina/GC-SCNA interlayer and GC-SCNA interlayer/trabecular coating were observed (Fig. 12). Trabecular coating and interlayer are composed by the same material (GC-SCNA) and, in correspondence of the contact areas, the interface between the two elements is not distinguishable.

The major drawback of GC-SCNA, as discussed in the sect. 3.3.2., is its low bioactivity. Indeed a high bioactivity, i.e. the ability to form an apatite layer after contact with biological fluids, is a crucial added value for bone tissue engineering biomedical implants. However, GC-SCNA trabecular coatings are not to be deemed unsuitable for promoting osteointegration: in fact, although exhibiting a moderate bioactive behaviour, they could still lead to osteogenesis *in vivo* by virtue of the key role played by their

bone-like porous architecture [24]. Looking at future research work, improvement of material bioactivity by means of surface functionalization [43] could also be a valuable option.

The second embodiment of the device, based on the use of a unique glass, is very attractive thanks to the ease of manufacturing; new bioactive glass formulations with low α are currently under investigation to find a satisfactory compromise between bioactivity, mechanical properties and coating ability of the glass chosen to fabricate both the interlayer and the trabecular coating.

4. Conclusions and perspectives

In spite of the advances of the last decades, minimally invasive, safe and long-lasting anchorage of prosthetic elements to the patient's bone still represents a great challenge that involves high cooperation among surgeons, biomechanical engineers and biomaterials researchers. In the present work, for the first time glass-derived scaffolds are proposed as osteointegrative trabecular coatings that are expected to induce biological fixation of prosthetic elements to bone. The feasibility of a trabecular coating on alumina exhibiting architectural features analogous to those of cancellous bone was successully demonstrated. The properties of the trabecular coating, in terms of mechanical behaviour and bioactivity potential, can be tailored by properly designing the composition of the starting glass. The present work is a pilot study that proves the applicability of trabecular coatings on flat (2-D) geometry but it should be considered that the majority of medical implants are characterized by complex, often curved shapes, like the semi-spherical one that is typical of the acetabular component of hip joint prostheses. Extension of the promising results achieved in the present work to curved geometry is not trivial and will require further research work in terms of glass composition design, scaffold shaping and coating techniques; the authors are currently working on these crucial issues in the course of a EU-funded project titled "Monoblock acetabular cup with trabecular-like coating" (MATCh, GA 286548), whose achievements will be the object of future publications. Utmost attention will be also devoted by the authors to the transfer of the most suitable manufacturing techniques from Lab-scale to industrial set-up. Under this perspective, the use of high-strength scaffolds as key components of implantable devices to promote

their osteointegration is highly innovative and could lead to the birth of a new generation of prostheses with relevant impacts from clinical, commercial and patient's life quality viewpoints. This device can allow ceramic/ceramic coupling, characterized by excellent wear resistance, and the presence of the 3-D trabecular glass-derived layer between cup and host bone can minimize the stiffness mismatch at their interface; therefore, the present research can potentially carry a significant innovation especially in the ceramic-on-ceramic joint prosthesis field.

Acknowledgements

This work was partly funded by the EU Network of Excellence project "Knowledge-based Multicomponent Materials for Durable and Safe Performance" (KMM-NoE, NMP3-CT-2004-502243). Prof. Milena Salvo is gratefully acknowledged for fruitful discussions.

References

[1] Soballe K, Overgaard S, Hansen ES, Brokstedt-Rasmussen H, Lind M, Bunger C. A review of ceramic coatings for implant fixation. J Long Term Eff Med Implants. 1999;9:131-51.

[2] Manley MT, Sutton K. Bearings of the future for total hip arthroplasty. J Arthroplasty. 2008;23:S47-S50.

[3] Hench LL, Anderson O. Bioactive glass coatings. In: Hench LL, Wilson J, editors. An introduction to bioceramics. Singapore: World Scientific; 1993. pp. 239-60.

[4] Verné E, Bosetti M, Vitale-Brovarone C, Moisescu C, Lupo F, Spriano S, Cannas M. Fluoroapatite glass-ceramic coatings on alumina: structural, mechanical and biological characterisation. Biomaterials. 2002;23:3395-403.

[5] Lopez-Esteban S, Saiz E, Fujino S, Oku T, Suganuma K, Tomsia AP. Bioactive glass coating for orthopaedic metallic implants. J Eur Ceram Soc. 2003,23:2921-30.

[6] Vitale-Brovarone C, Verné E. SiO_2-CaO-K_2O coatings on alumina and Ti6Al4V substrates for biomedical applications. J Mater Sci: Mater Med. 2005;16:863-71.

[7] Verné E, Vitale-Brovarone C, Moisescu C. Glazing of alumina by a fluoroapatite-containing glass-ceramic. J Mater Sci. 2005;40:1209-15.

[8] Bigi A, Boanini E, Bracci B, Facchini A, Panzavolta S, Segatti F, Sturba L. Monocrystalline hydroxyapatite coatings on titanium: a new fast biomimetic method. Biomaterials. 2005;26:4085-9.

[9] Fathi MH, Doostmohammadi A. Bioactive glass nanopowder and bioglass coating for biocompatibility improvement of metallic implant. J Mater Processing Technol. 2009;209:1385-91.

[10] Wang X, Li X, Onuma K, Ito A, Sogo Y, Kosuge K, Oyane A. Mesoporous bioactive glass coatings on stainless steel for enhanced cell activity, cytoskeletal organization and AsMg immobilization. J Mater Chem. 2010;20:6437-45.

[11] Sun L, Berndt CC, Gross KA, Kucuk A. Material fundamentals and clinical performance of plasma-sprayed hydroxyapatite coatings: a review. J Biomed Mater Res: Appl Biomater. 2001;58:570-92.

[12] Yang Y, Kim KH, Ong JL. A review on calcium phosphate coatings produced using a sputtering process – an alternative to plasma spraying. Biomaterials. 2005,26:327-37.

[13] Boccaccini AR, Keim S, Ma R, Li Y, Zhitomirsky I. Electrophoretic deposition of biomaterials. J R Soc Interface. 2010;7:S581-S613.

[14] Klein CPAT, Wolke JGC, De Groot K. Stability of calcium phosphate ceramics and plasma sprayed coatings. In: Hench LL, Wilson J, editors. An introduction to bioceramics. Singapore: World Scientific; 1993. pp. 199-222.

[15] Dorozhkin SV. Bioceramics of calcium orthophosphates. Biomaterials. 2010;31:1465-85.

[16] Tomsia AP, Saiz E, Song J, Bertozzi CR. Biomimetic bonelike composites and novel bioactive glass coatings. Adv Eng Mater. 2005;7:999-1004.

[17] Hench LL, Splinter RJ, Allen WC, Greenlee TK. Bonding mechanisms at the interface of ceramic prosthetic materials. J Biomed Mater Res. 1972;2:117-41.

[18] Hench LL. The story of Bioglass®. J Mater Sci: Mater Med. 2006;17:967-78.

[19] Hench LL. Genetic design of bioactive glasses. J Eur Ceram Soc. 2009;29:1257-65.

[20] Hoppe A, Guldal NS, Boccaccini AR. A review of the biological response to ionic dissolution products from bioactive glasses and glass-ceramics. Biomaterials. 2011;32:2757-74.

[21] Foppiano S, Marshall SJ, Marshall GW, Saiz E, Tomsia AP. Bioactive glass coatings affect the behavior of ostoblast-like cells. Acta Biomaterialia. 2007;3:765-71.

[22] Gerhardt LC, Boccaccini AR. Bioactive glass and glass-ceramic scaffolds for bone tissue engineering. Materials. 2010;3:3867-910.

[23] Baino F, Vitale-Brovarone C. Three-dimensional glass-derived scaffolds for bone tissue engineering: current trends and forecasts for the future. J Biomed Mater Res A. 2011;97:514-35.

[24] Karageorgiou V, Kaplan D. Porosity of 3D biomaterial scaffolds and osteogenesis. Biomaterials. 2005;26:5474-91.

[25] Verné E, Vitale-Brovarone C, Robiglio L, Baino F. Single-piece ceramic prosthesis elements. WO 2008/146322 A2.

[26] Vitale-Brovarone C, Verné E, Robiglio L, Appendino P, Bassi F, Martinasso G, Muzio G, Canuto R. Development of glass-ceramic scaffolds for bone tissue engineering: Characterisation, proliferation of human osteoblasts and nodule formation. Acta Biomater. 2007;3:199-208.

[27] Vitale-Brovarone C, Baino F, Verné E. High strength bioactive glass-ceramic scaffolds for bone regeneration. J Mater Sci: Mater Med. 2009;20:643-53.

[28] Verné E, Miola M, Vitale-Brovarone C, Cannas M, Gatti S, Fucale G, Maina G, Massé A, Di Nunzio S. Surface silver-doping of biocompatibile glass to induce antibacterial properties. Part I: massive glass. J Mater Sci: Mater Med. 2009;20:733-40.

[29] Baino F, Ferraris M, Bretcanu O, Verné E, Vitale-Brovarone C. Optimization of composition, structure and mechanical strength of bioactive 3-D glass-ceramic scaffolds for bone substitution. J Biomater Appl. (in press). DOI: 10.1177/0885328211429193.

[30] Priven AI. General method for calculating the properties of oxide glass and glass forming melts from their composition and temperature. Glass Technol. 2004;45:244-254.

[31] Chalker PR, Bull SJ, Rickerby DS. A review of the methods for the evaluation of coating-substrate adhesion. Mater Sci Eng A. 1991;140:583-92.

[32] Gomez-Vega JM, Saiz E, Tomsia AP, Marshall GW, Marshall SJ. Bioactive glass coatings with hydroxyapatite and Bioglass® particle on Ti-based implants. 1. Processing. Biomaterials. 2000;21:105-11.

[33] ASTM F1538-03 (2009): Standard Specification for Glass and Glass Ceramic Biomaterials for implantation.

[34] ASTM C633-01 (2008): Standard Test Method for Adhesion or Cohesion Strength of Thermal Spray Coatings.

[35] Kokubo T, Takadama H. How useful is SBF in predicting in vivo bone bioactivity?. Biomaterials. 2006;27:2907-15.

[36] Kokubo T, Ito S, Sakka S, Yamamuro T. Formation of a high-strength bioactive glass-ceramic in the system MgO-CaO-SiO_2-P_2O_5. J Mater Sci. 1986;21:536-40.

[37] Xue W, Liu X, Zheng XB, Ding C. In vivo evaluation of plasma-sprayed wollastonite coating. Biomaterials. 2005;26:3455-60.

[38] Erol M, Kucukbayrak S, Ersoy-Mericboyu A. Influence of particle size on the crystallization kinetics of glasses produced from waste materials. J Non-Cryst Solids. 2011;357:211-9.

[39] ISO 13779-4 (2002): Implants for surgery - Hydroxyapatite - Part 4: Determination of coating adhesion strength.

[40] Chen QZ, Thompson ID, Boccaccini AR. 45S5 Bioglass®-derived glass-ceramic scaffolds for bone tissue engineering. Biomaterials. 2006;27:2414-25.

[41] Bretcanu O, Chen Q, Misra SK, Boccaccini AR, Verné E, Vitale-Brovarone C. Biodegradable polymer coated 45S5 Bioglass-derived glass-ceramic scaffolds for bone tissue engineering. Glass Tech Eur J: Glass Sci Tech A. 2007;48:227-34.

[42] Kokubo T, Kushitani H, Ohtsuki C, Sakka S, Yamamuro T. Effects of ions dissolved from bioactive glass-ceramics on surface apatite formation. J Mater Sci: Mater Med. 1993;4:1-4.

[43] Verné E, Ferraris S, Vitale-Brovarone C, Spriano S, Bianchi CL, Naldoni A, Morra M, Cassinelli C. Alkaline phosphatase grafting on bioactive glasses and glass-ceramics. Acta Biomater. 2010;6:229-40.

Tables

Table 1

Features of the glasses used for manufacturing the samples.

Glass	Composition (%mol.)							Melting conditions (heating rate: 10 °C min^{-1})	α ($\times 10^{-6}$ °C^{-1})
	SiO_2	P_2O_5	CaO	Na_2O	MgO	K_2O	Al_2O_3		
SCK	50	-	44	-	-	6	-	1500 °C/1 h	10.06
CEL2	45	3	26	15	7	4	-	1400 °C/1 h	12.83
SCNA	57	-	34	6	-	-	3	1550 °C/1 h	8.70

Figure

Fig. 1. Scheme of the innovative acetabular cup disclosed in the patent deposited by the authors [36]: this monoblock ceramic implant is constituted by three elements: (i) a bioinert ceramic substrate, that articulates directly with the (prosthetic) femur head; (ii) a bioactive trabecular coating, i.e. a glass-derived scaffold, that aims at promoting implant osteointegration to patient's pelvis bone; (iii) a glass-derived (pore-free or minimally porous) interlayer, able to improve the adhesion between alumina substrate (cup) and trabecular coating (scaffold).

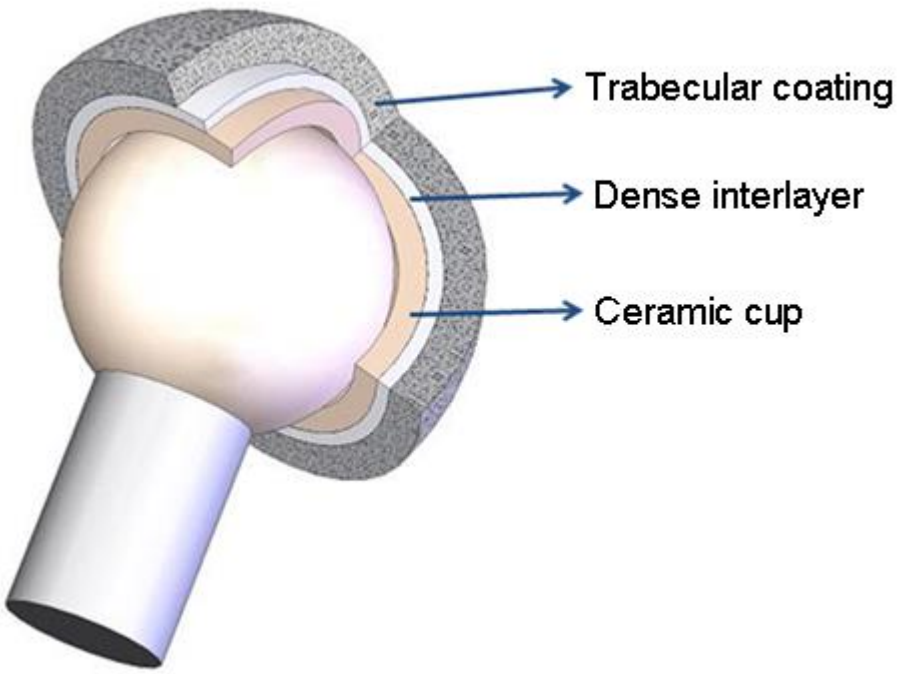

Fig. 2. Different strategies adopted for fabricating complete plane samples; note that methods I and II involve a graded GC-SCK/GC-CEL2 interlayer between alumina substrate and trabecular coating.

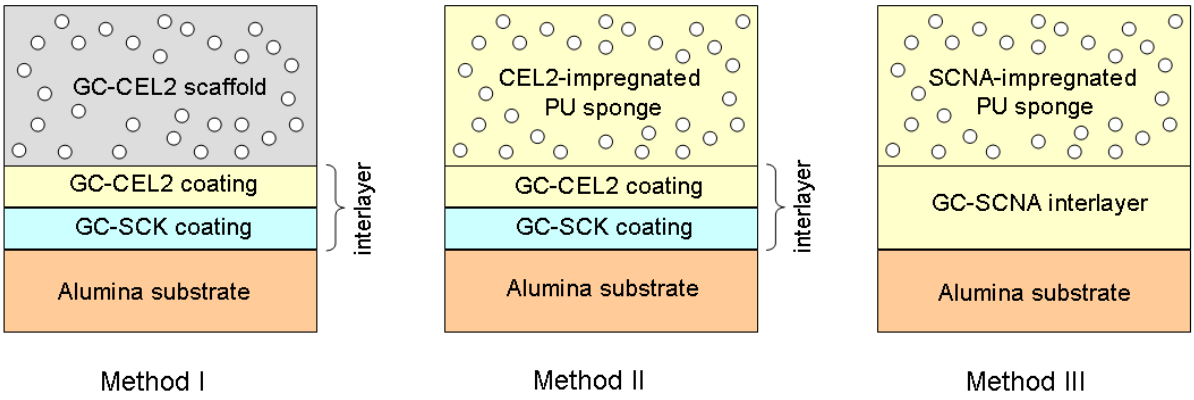

Fig. 3. GC-SCK coatings manufactured by using SCK powders belonging to different size ranges: (a) below 32 μm, (b) within 32-75 μm, (c) and (d) within 75-106 μm.

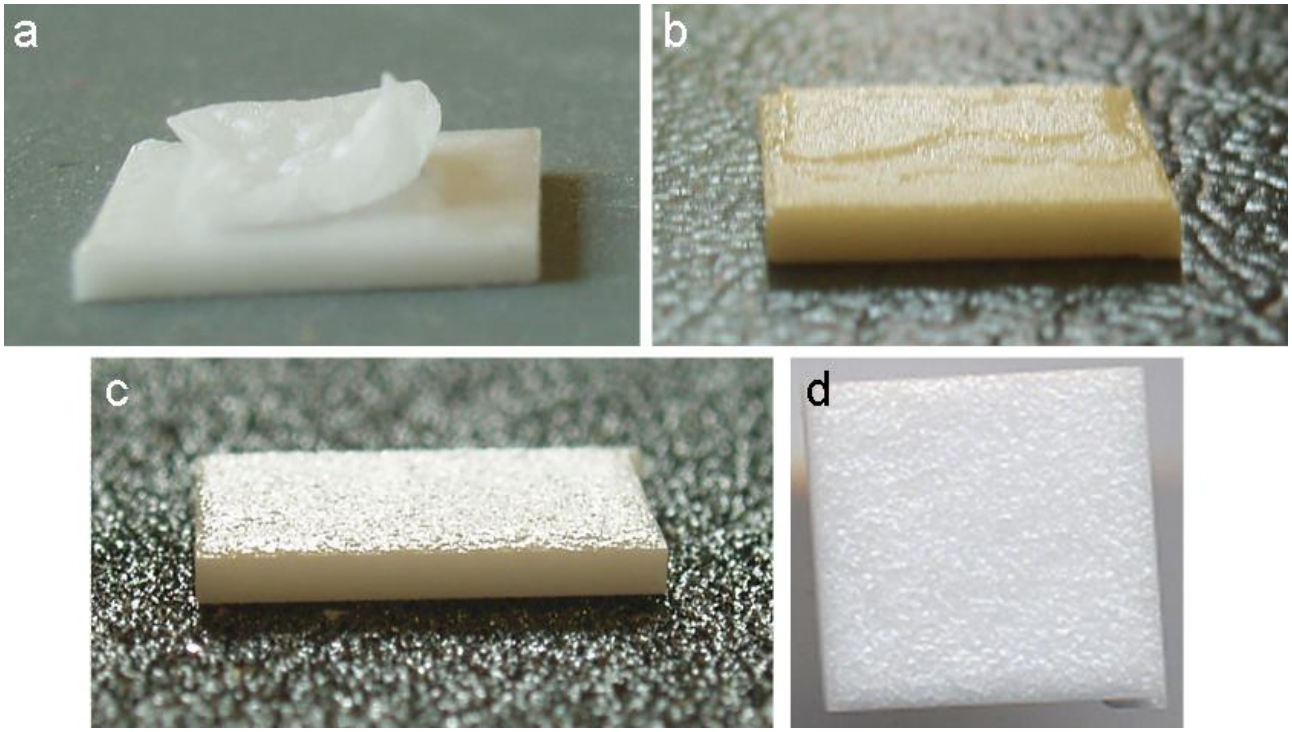

Fig. 4. GC-CEL2/GC-SCK coatings: (a) SEM investigation (back-scattering); compositional analysis on (b) the black circle and (c) the black square areas.

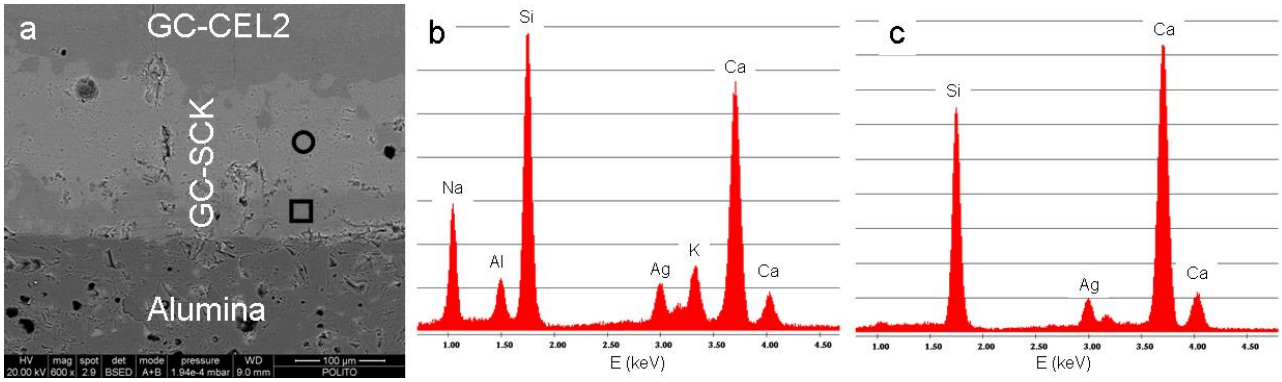

Fig. 5. Microindentation at the alumina/GC-SCK interface (load: 5 N): the cracks propagated along the GC-SCK coating and the interface did not delaminate.

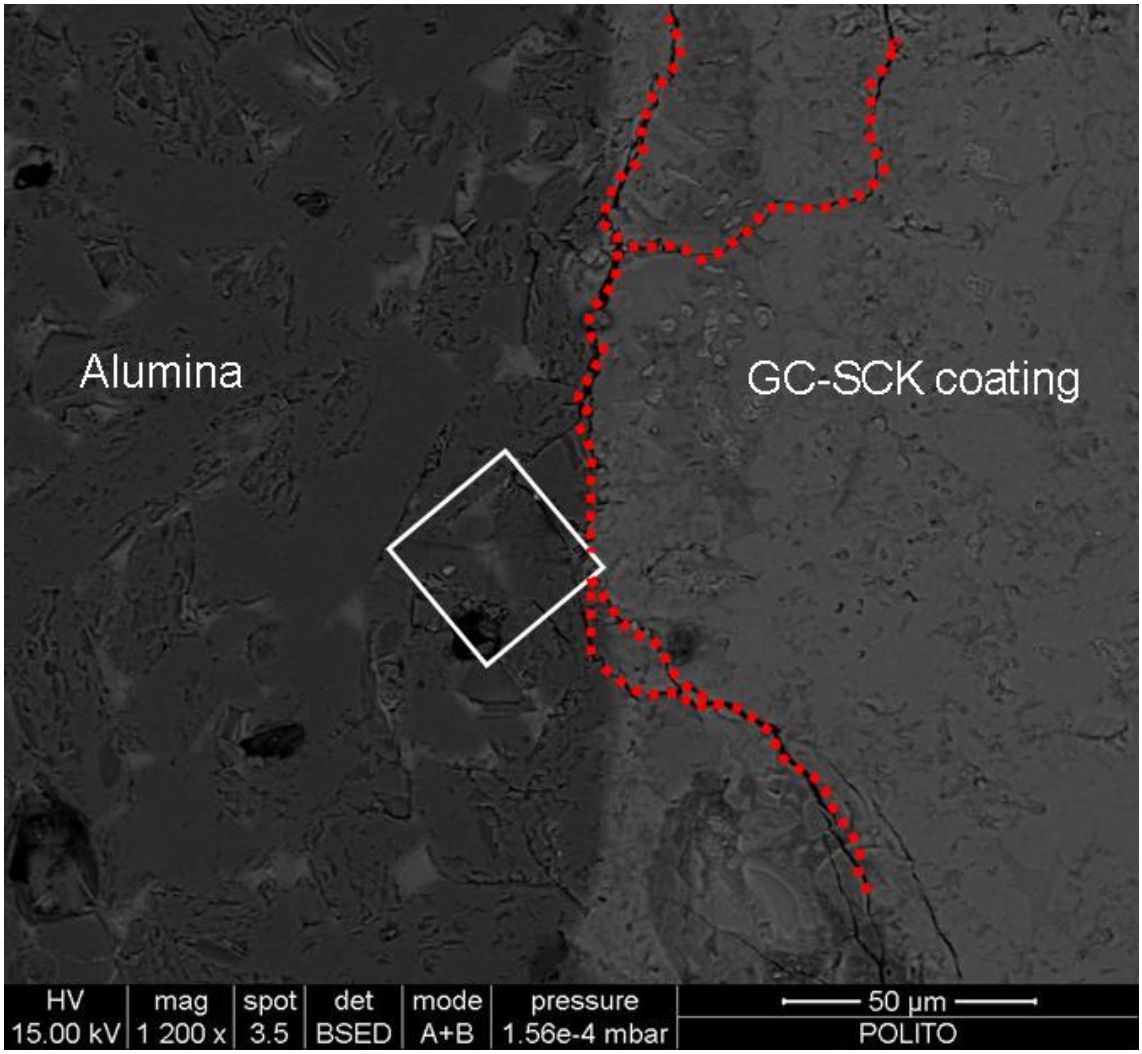

Fig. 6. SEM micrographs, at different magnifications, of the samples fabricated by (a) method I (the white circles emphasize the regions of discontinuity between GC-CEL2 scaffold and underlying coating) and (b, c) method II.

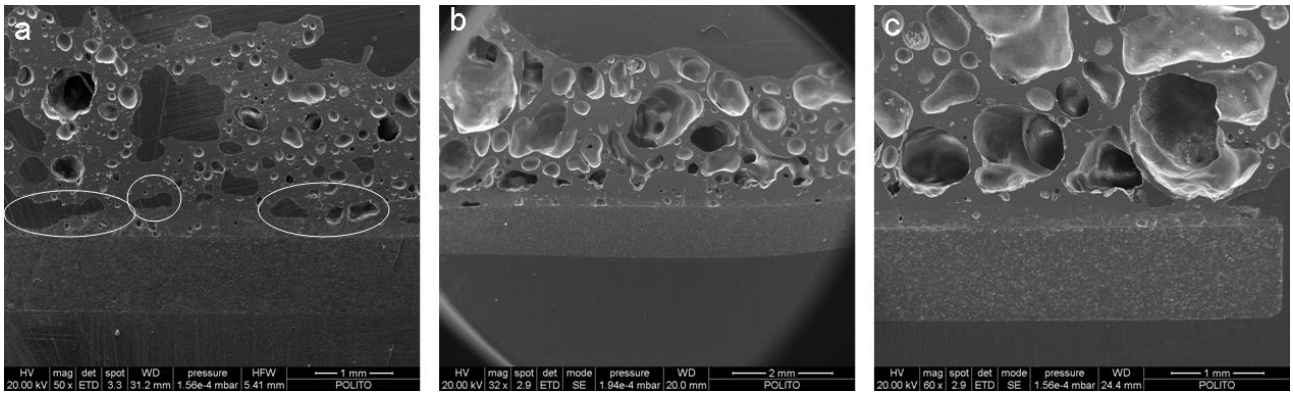

Fig. 7. *In vitro* bioactivity after soaking in SBF (SEM analysis): (a) complete sample overview after soaking for 1 week; (b) apatite layer formed on pores walls in the inner region of the trabecular coating; (c) micrograph of the whole sample after soaking for 1 month (the pores walls where the growth of apatite is more evident are emphasized).

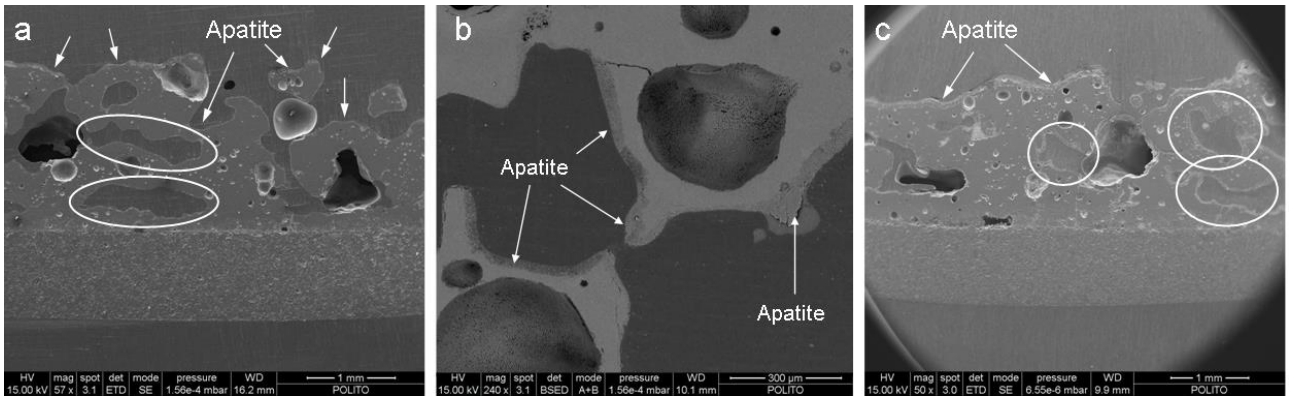

Fig. 8. SEM micrographs GC-SCNA coating on alumina plates: (a) sample overview and (b) detail of the substrate/coating interface.

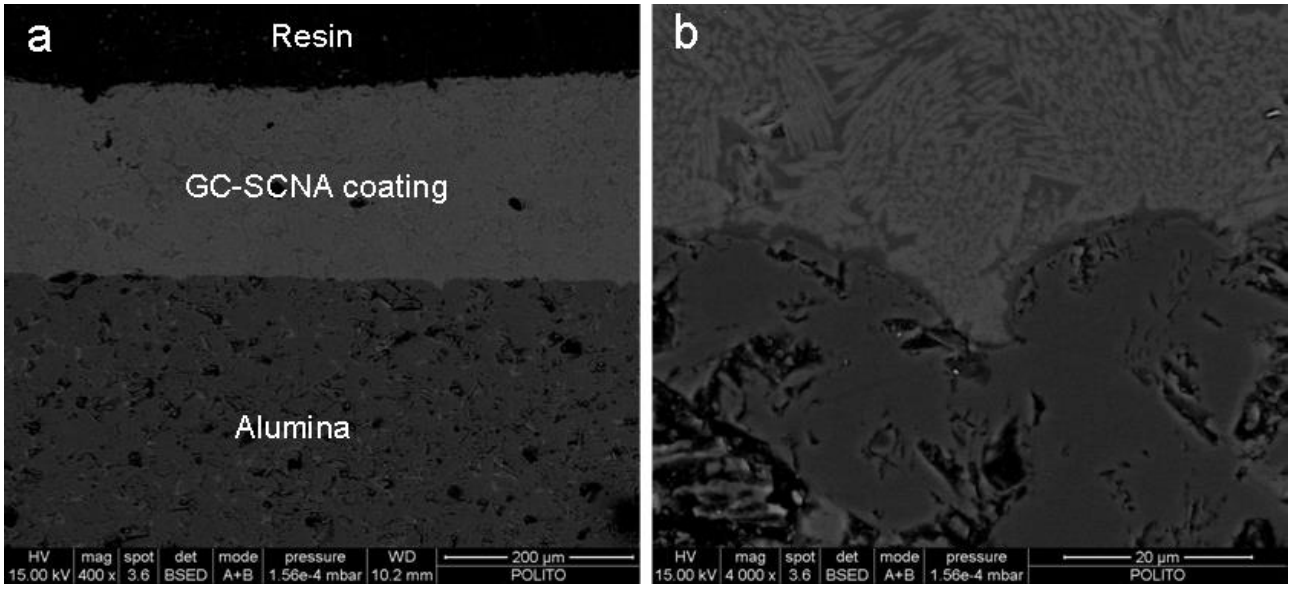

Fig. 9. Microindentation at the alumina/GC-SCNA interface (load: 5 N); the white arrows "follow" the direction of crack propagation.

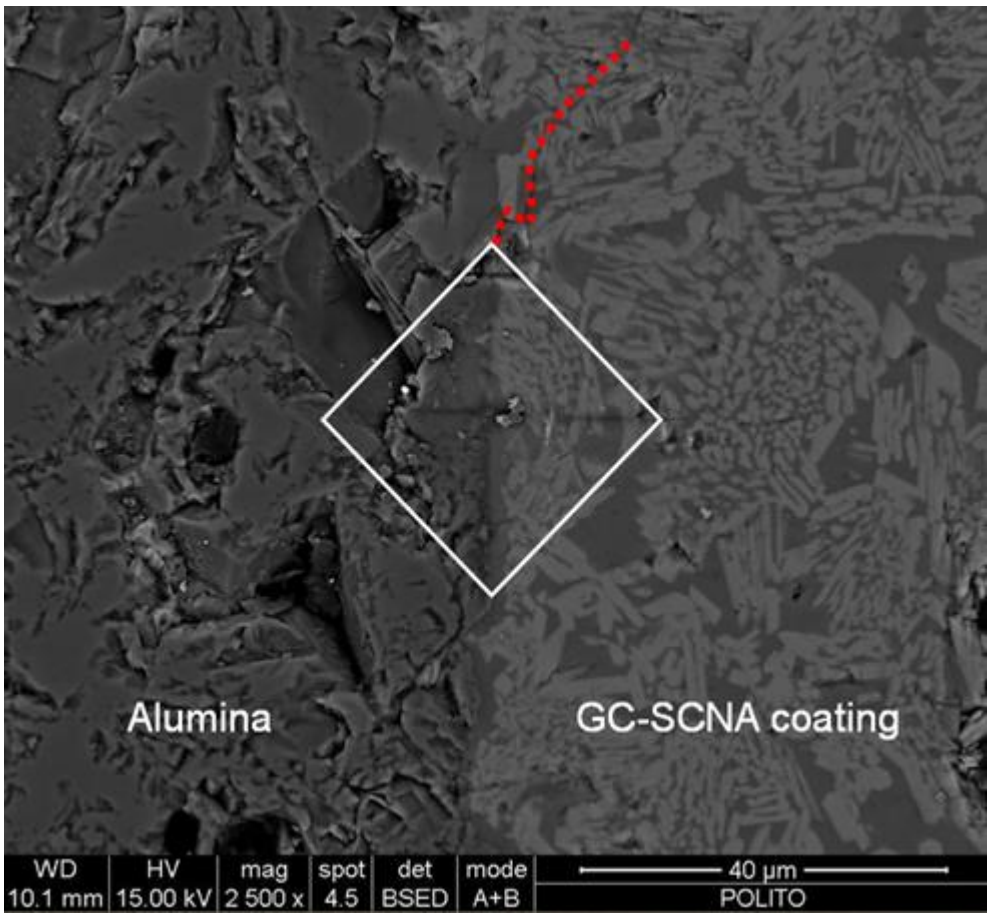

Fig. 10. GC-SCNA scaffolds: (a,b) SEM micrographs of scaffold cross-section section at different magnifications; (c) needle-shaped wollastonite crystals on a scaffold strut.

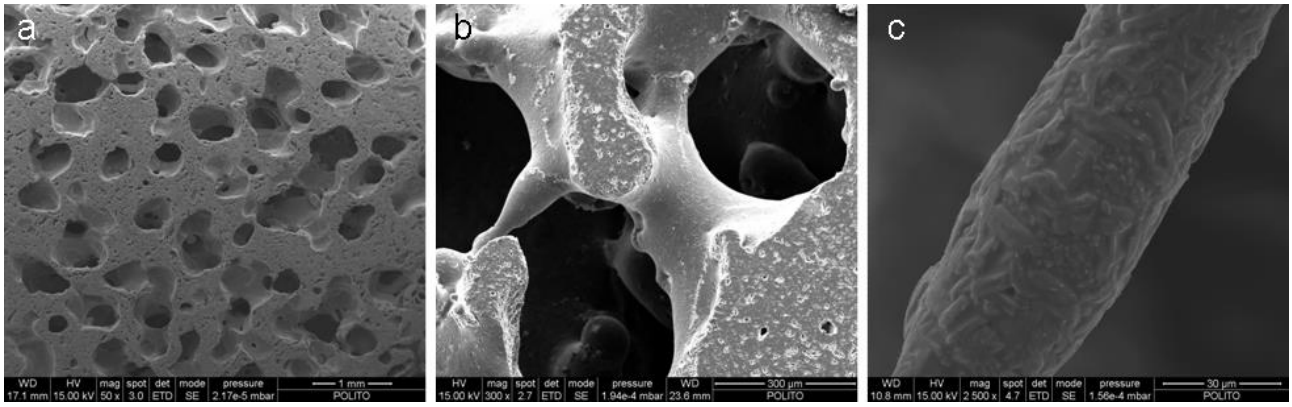

Fig. 11. High-magnification SEM micrograph of GC-SCNA scaffold surface after soaking for 7 days in SBF.

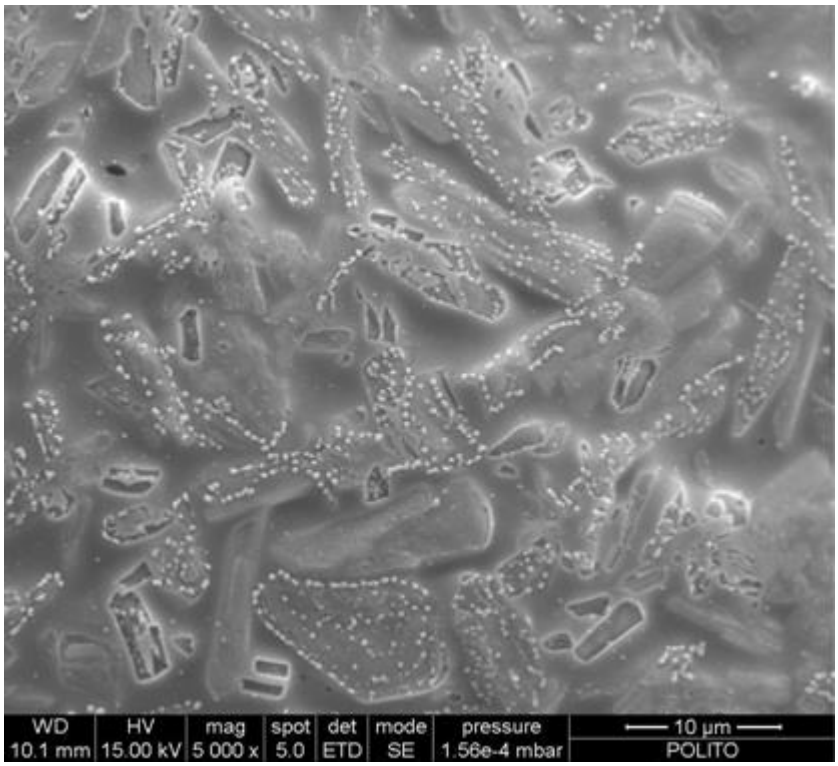

Fig. 12. SEM micrograph of a sample produced by Method III (second embodiment).